Chemical composition dependences of the acoustical physical constants of LiNbO3 and LiTaO3 single crystals

doi: 10.1063/1.1467608

Chemical composition dependences of the acoustical physical constants of $LiNbO_3$ and $LiTaO_3$ single crystals

J. Kushibiki,[a] I. Takanaga, S. Komatsuzaki, and T. Ujiie
Department of Electrical Engineering, Tohoku University, Sendai 980-8579, Japan

(Received 4 September 2001; accepted for publication 13 February 2002)

We determined all the independent components of the acoustical physical constants (elastic constant, piezoelectric constant, dielectric constant, and density) of $LiNbO_3$ and $LiTaO_3$ crystals grown from the melts of three different starting materials with the Li_2O contents set to 48.0, 48.5, and 49.0 mol %, and obtained the chemical composition dependences of the constants of each single crystal around the congruent composition. All the constants as well as the measured longitudinal, shear, and leaky surface acoustic wave (LSAW) velocities varied linearly with the composition ratios in the experimental range. The composition dependences of the LSAW velocities for the 128° YX-$LiNbO_3$, X-112° Y-$LiTaO_3$, and 36° YX-$LiTaO_3$ substrates, previously obtained by line-focus-beam acoustic microscopy, were well matched with the calculated ones using the constants determined. Therefore the data of the composition dependences of the determined constants enable us to easily prepare the calibration lines for evaluating the crystals for any arbitrarily cut specimen surfaces, wave propagation directions, and modes by numerical calculations. © *2002 American Institute of Physics.* [DOI: 10.1063/1.1467608]

I. INTRODUCTION

$LiNbO_3$ (Refs. 1 and 2) and $LiTaO_3$ (Refs. 1, 3, and 4) single crystals are widely used as material for bulk acoustic wave (BAW) devices and surface acoustic wave (SAW) devices. The rapid development of mobile communication devices in recent years has increased the demand for even higher quality single crystals. The chemical composition differences and variations in crystals most influence the quality of single-crystal wafer substrates, particularly the uniformity of their physical and chemical characteristics.[2–4] It is thus important to produce crystal wafer substrates for SAW devices having highly uniform acoustic properties in order to improve the device yield rate. Therefore it is necessary to evaluate the variations in acoustic properties caused by the variations in chemical composition and to feed that information back to the crystal growth conditions.

Ultrasonic micro-spectroscopy (UMS) technology enables accurate analysis and evaluation of the acoustic properties of various materials using the line-focus-beam (LFB) acoustic microscopy system[5,6] and the bulk ultrasonic spectroscopy system.[7,8] This technology has been applied to various materials, including $LiNbO_3$ and $LiTaO_3$ single crystals, and its usefulness has been demonstrated.[9–12] The acoustical physical constants of materials (elastic constant c^E, piezoelectric constant e, dielectric constant ε^S, and density ρ) of commercially available SAW-grade $LiNbO_3$ and $LiTaO_3$ single crystals, which have a nearly congruent chemical composition, have also been accurately measured recently, giving BAW and SAW velocities with four significant figures.[13]

To evaluate and analyze $LiNbO_3$ and $LiTaO_3$ single crystals using UMS technology, we must prepare calibration lines of the acoustic properties to be measured against the chemical composition to be evaluated. For example, when implementing an evaluation with the leaky surface acoustic wave (LSAW) velocities measured by an LFB system, we must obtain the relationship between the chemical compositions and LSAW velocities by preparing several substrate specimens with different chemical compositions for a required cut surface and then measuring the LSAW velocities on each specimen. It is very time-consuming. Chemical compositions of 127.86° rotated Y-cut X-propagating (128° YX)-$LiNbO_3$ (Ref. 14), X-cut 112.2° rotated Y-propagating (X-112° Y)-$LiTaO_3$ (Ref. 15), and 36° YX-$LiTaO_3$ (Ref. 16) substrates have been so far evaluated according to such experimental procedures.[11,17,18] In addition, we are unable to directly evaluate the SAW velocities, which are closely related to the characteristics of the SAW devices, and, in particular, the pseudo surface acoustic wave (PSAW) velocities of SH type, since LFB acoustic microscopy enables measuring only the Rayleigh propagation mode on the water-loaded specimen surfaces from its principle of operation.

If we could have all independent components of the acoustical physical constants of these crystals as a function of the chemical composition ratio, we could obtain chemical composition dependences of the acoustic properties for an arbitrarily cut specimen surface, wave propagation direction, and mode by numerical calculations, enabling a very efficient evaluation. Furthermore, the calculated relationships between LSAW velocities and SAW velocities can be easily obtained. We could then evaluate SAW velocities from measured LSAW velocities. However, the previously published values of the acoustical physical constants of $LiNbO_3$ and $LiTaO_3$ single crystals were determined only for a nearly congruent chemical composition;[13,19–21] there are no reports

[a]Electronic mail: kushi@ecei.tohoku.ac.jp

concerning the chemical composition dependences of the constants.

In this article we determine the chemical composition dependences of the constants for $LiNbO_3$ and $LiTaO_3$ crystals around the congruent composition.

II. DETERMINATION PROCEDURE

$LiNbO_3$ and $LiTaO_3$ single crystals belong to class 3m of the trigonal system and have a total of 13 independent acoustical physical constants, which consist of six elastic stiffness constants at constant electric field [$c_{11}^E(=c_{12}^E+2c_{66}^E)$, c_{12}^E, c_{13}^E, c_{14}^E, c_{33}^E, and c_{44}^E], four piezoelectric stress constants (e_{15}, e_{22}, e_{31}, and e_{33}), two dielectric constants at constant strain (ε_{11}^S and ε_{33}^S), and the density (ρ). Of these, the two dielectric constants and density must be measured independently when considering the relationship between acoustic velocities and acoustical physical constants. Therefore the six elastic stiffness constants and four piezoelectric constants can be determined from ten measured velocities.

In our procedure of determining the acoustical physical constants, some of the constants are determined in advance using velocities of bulk acoustic waves, whose relation to the acoustical physical constants is relatively simple, so that more accurate determination can be made in combination with LSAW velocities measured by the LFB system.[22]

The constants c_{11}^E, c_{44}^E, and c_{66}^E can be determined independently from the measured density and three velocities, viz., the *X*-axis longitudinal velocity V_{Xl}, the *Z*-axis shear velocity V_{Zs}, and the *Y*-axis shear velocity with *X*-axis polarized particle displacement V_{YsX} for the bulk acoustic waves propagating along the crystallographic *X*, *Y*, and *Z* axes, as being expressed in the following equations:

$$\rho V_{Xl}^2 = c_{11}^E, \tag{1}$$

$$\rho V_{Zs}^2 = c_{44}^E, \text{ and} \tag{2}$$

$$\rho V_{YsX}^2 = c_{66}^E = (c_{11}^E - c_{12}^E)/2. \tag{3}$$

And the constant c_{14}^E can be determined from the determined c_{44}^E and c_{66}^E and the rotated *Y*-axis shear velocity with *X*-axis polarized particle displacement V_{rYsX}, measured for a rotated *Y*-cut plate specimen as expressed by

$$\rho V_{rYsX}^2 = c_{14}^E \sin 2\theta + c_{44}^E \sin^2\theta + c_{66}^E \cos^2\theta, \tag{4}$$

where θ is the rotation angle about the *X* axis from the *Y* axis to the *Z* axis. For this procedure, to determine c_{14}^E with high accuracy, we must select a rotated *Y*-cut plate specimen that shows the largest c_{14}^E dependence on the velocity change in V_{rYsX}.[13]

Furthermore, the rotated *Y*-axis longitudinal velocities V_{rYl} for rotated *Y*-cut plates including the *Y*- and *Z*-cut plates are related to the acoustical physical constants in the following equation:

$$\begin{vmatrix} c_{11}^{E'} - \rho V_{rYl}^2 & c_{16}^{E'} & e_{11}' \\ c_{16}^{E'} & c_{66}^{E'} - \rho V_{rYl}^2 & e_{16}' \\ e_{11}' & e_{16}' & -\varepsilon_{11}^S \end{vmatrix} = 0. \tag{5}$$

The primed constants indicate that the constants have been subjected to coordinate transformation for the desired propagation direction. The constants $c_{11}^{E'}$, $c_{16}^{E'}$, and $c_{66}^{E'}$ are all functions of the five elastic constants other than c_{12}^E, and the rotation angle θ for the rotated *Y*-cut specimen. Both e_{11}' and e_{16}' are functions of the four piezoelectric constants and θ, and $\varepsilon_{11}^{S'}$ is a function of the two dielectric constants and θ.

Also, we employ LSAW velocities for the three rotated *Y*-cut plate specimens used for the longitudinal velocity measurements. As a proper propagation direction for accurate measurements of LSAW velocities, we take LSAWs of a pure Rayleigh mode propagating in the 90° *X*-axis direction on the rotated *Y*-cut specimen. The relation between the LSAW velocity V_{LSAW} measured for the rotated *Y*-cut 90° *X*-propagating specimen and the acoustical physical constants are represented as

$$\begin{vmatrix} c_{11}^{E'} + 2j\beta c_{15}^{E'} - \beta^2 c_{55}^{E'} - \rho V_{\mathrm{LSAW}}^{*2} & c_{15}^{E'} + j\beta(c_{13}^{E'} + c_{55}^{E'}) - \beta^2 c_{35}^{E'} & e_{11}' + j\beta(e_{31}' + e_{15}') - \beta^2 e_{35}' \\ c_{15}^{E'} + j\beta(c_{13}^{E'} + c_{55}^{E'}) - \beta^2 c_{35}^{E'} & c_{55}^{E'} + 2j\beta c_{35}^{E'} - \beta^2 c_{33}^{E'} - \rho V_{\mathrm{LSAW}}^{*2} & e_{15}' + j\beta(e_{13}' + e_{35}') - \beta^2 e_{33}' \\ e_{11}' + j\beta(e_{31}' + e_{15}') - \beta^2 e_{35}' & e_{15}' + j\beta(e_{13}' + e_{35}') - \beta^2 e_{33}' & -(\varepsilon_{11}^{S'} + 2j\beta\varepsilon_{13}^{S'} - \beta^2 \varepsilon_{33}^{S'}) \end{vmatrix} = 0. \tag{6}$$

In this equation, V_{LSAW}^* is the complex velocity and β is the component of the wave number in the depth direction of the substrate normalized by the wave number of the surface waves in the propagation direction, satisfying the boundary conditions at the interface between the water and the specimen surface.[23] The constants $c_{11}^{E'}$, $c_{13}^{E'}$, $c_{15}^{E'}$, $c_{33}^{E'}$, $c_{35}^{E'}$, and $c_{55}^{E'}$ are all functions of the five elastic constants other than c_{12}^E, and the rotation angles θ for the rotated *Y*-cut specimens; e_{11}', e_{13}', e_{15}', e_{31}', e_{33}', and e_{35}' are functions of the four piezoelectric constants and θ; and $\varepsilon_{11}^{S'}$, $\varepsilon_{13}^{S'}$, and $\varepsilon_{33}^{S'}$ are functions of the two dielectric constants and θ.

Therefore the six constants, c_{13}^E, c_{33}^E, e_{15}, e_{22}, e_{31}, and e_{33}, are determined by selecting six combinations of propagation directions and wave modes that satisfy Eq. (5) or Eq. (6) and solving the simultaneous equations.

Following the procedure described above, all the acoustical physical constants can be determined from ten measured velocities: the longitudinal velocities for all four specimens; and the *X*-axis polarized shear velocities and the

TABLE I. Measured Curie temperatures and estimated Li_2O concentrations of $LiNbO_3$ and $LiTaO_3$ crystals used in experiments.

	Prepared Li_2O concentration (mol %)	Curie temperature (°C)	Analyzed Li_2O concentration (mol %)
$LiNbO_3$	48.0	1124.1	48.28
	48.5	1130.0	48.41
	49.0	1136.2	48.55
$LiTaO_3$	48.0	595.8	48.35
	48.5	601.8	48.50
	49.0	607.7	48.66

90° *X*-axis propagating LSAW velocities for the *Y*-cut, *Z*-cut, and rotated *Y*-cut specimens.[22]

III. PREPARATION OF SPECIMENS

We prepared three crystal ingots each for $LiNbO_3$ and $LiTaO_3$ grown from melts of starting materials with Li_2O content set to 48.0, 48.5, and 49.0 mol %. Three-inch diameter crystals were grown by the Czochralski method (Yamaju Ceramics Co., Ltd., Seto, Japan). The $LiNbO_3$ crystals were pulled along the *Z*-axis direction; the $LiTaO_3$ crystals along the *Y*-axis direction.

The chemical composition was determined from the Curie temperatures[24,25] measured by the differential thermal analysis (DTA) method for specimens cut near the central portion of the growing axis of each crystal. The results are listed in Table I. Assuming that the measurement accuracy of the Curie temperatures was 1 °C, the corresponding variation in chemical composition ratio was estimated to be 0.02 Li_2O mol % for the $LiNbO_3$ crystals and 0.03 Li_2O mol % for the $LiTaO_3$ crystals.

Figure 1 shows the configuration of specimen preparation for each of the $LiNbO_3$ and $LiTaO_3$ crystals used for determining the constants. Each specimen was prepared so that the center of the specimen, corresponding to the velocity measurement position, was contained in the circular disk plane perpendicular to the crystal growth axis. This preparation method effectively reduces differences in chemical composition at velocity measurement positions among the specimens prepared from the same crystal, as single crystals grown from melts with noncongruent compositions have gradients in chemical composition along the growth axis direction but are almost uniform along the diameter direction.[10]

Three principal *X*-, *Y*-, and *Z*-cut specimens and a rotated *Y*-cut specimen were prepared from each crystal boule based on the literature.[22] The (104) [127.85° rotated *Y* (128° *Y*)-cut] plate for the $LiNbO_3$ crystals and the (012) [32.93° rotated *Y* (33° *Y*)-cut] plate for the $LiTaO_3$ crystals were selected from the crystalline planes cited in the American Society for Testing and Materials (ASTM) cards (No. 20-631 for $LiNbO_3$ and No. 29-836 for $LiTaO_3$) that could be used for most accurately determining the constants.

Every specimen was optically polished on both sides to a thickness of 3 to 4 mm to eliminate influences from the waves reflected from the back surface of the specimen during the measurement of LSAW velocities by LFB acoustic microscopy [26] and so that bulk velocities could be measured using the pulse measurement method. The inclination angles between the crystalline planes and the specimen surfaces were measured on all the specimens and were found to be 0.1° maximum by X-ray analysis. Any change in velocity caused by such inclination can be compensated through numerical calculations.

IV. MEASURING METHODS

A. BAW velocity

We measured BAW velocities by the ultrasonic pulse interference method using radio frequency (rf) tone burst signals.[8] Figure 2 shows the setup for the experiment to measure the BAW velocities. Two plane-wave ultrasonic devices were used, consisting of a cylindrical buffer rod of synthetic silica (SiO_2) glass with a ZnO film transducer for longitudinal waves or an *X*-cut $LiNbO_3$ transducer for shear waves fabricated on one end of the rod. Pure water was used as the coupling material for the longitudinal waves, and the rod and specimen were bonded using salol (phenyl salicylate) for the shear waves. Ultrasonic waves converted from electrical rf pulse signals by the transducer propagate through the rod, coupling material, and specimen, and are then transmitted across or reflected at the boundaries. The interference wave form shown in Fig. 3 can be obtained by superposing the pulse signals reflected from the front surface of the specimen, V_1, and those reflected from the back surface, V_2, in the time domain using the double-pulse method and by sweeping the carrier frequency. The BAW velocity *V* is determined from the frequency interval in the interference wave form, Δf, and the thickness of the specimen, *h*, using the following equation:

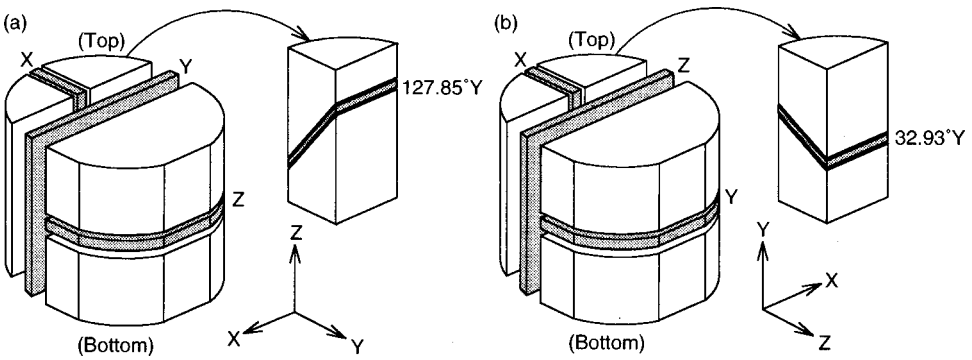

FIG. 1. Configurations of specimen preparation of $LiNbO_3$ and $LiTaO_3$ crystals. (a) $LiNbO_3$ and (b) $LiTaO_3$.

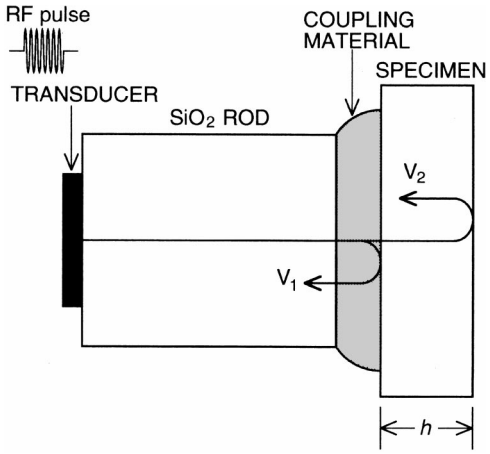

FIG. 2. Experimental arrangement for bulk ultrasonic velocity measurements by the pulse interference method.

$$V = 2\Delta f h. \tag{7}$$

The specimen thickness was measured with an accuracy of ± 0.10 μm using a digital length gauging system. In measuring the shear wave velocities, the signals reflected from the rod end and those reflected from the front surface of the specimen cannot be separated in the time domain. The influence of the phase change in the bonding layer on the acoustic velocity is therefore compensated through numerical calculations. The accuracy is ± 0.3 m/s for the longitudinal and shear velocities.

B. LSAW velocity

LSAW velocities are measured by the most recent LFB ultrasonic material characterization (UMC) system.[6] The LFB-UMC system enables us to measure the phase velocity of LSAWs propagating on the water-loaded specimen surface by analyzing V(z) curves obtained when varying the relative distance z between the LFB ultrasonic device and the specimen,[5] as illustrated in Fig. 4, which represents the principle of forming the V(z) curve. The ultrasonic device consists of a Z-cut sapphire rod with a ZnO piezoelectric film transducer on the top face and a cylindrical acoustic lens on the bottom face. Components No. 0 and No. 1 in the figure interfere with each other when the relative distance z is varied. An interference wave form of the V(z) curve is then obtained, as shown in Fig. 5. The LSAW velocity V_{LSAW} can be obtained from the oscillation interval Δz in the interference wave form using the following equation:

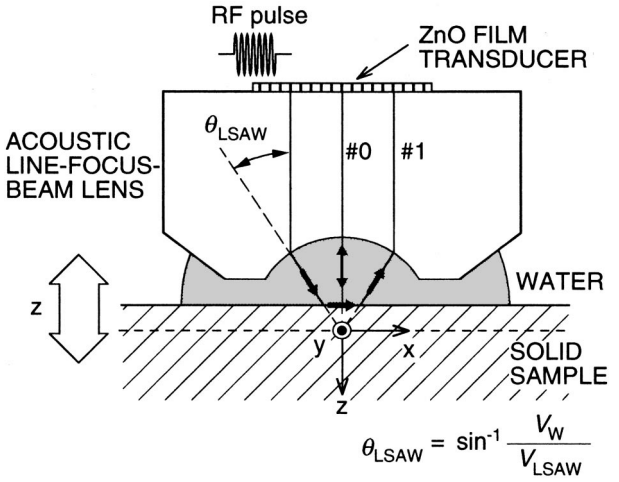

FIG. 4. Cross section of the experimental setup of the LFB ultrasonic device and specimen system for V(z) curve measurements.

$$V_{\mathrm{LSAW}} = \frac{V_W}{\sqrt{1-\left(1-\dfrac{V_W}{2f\Delta z}\right)^2}}. \tag{8}$$

Here, V_W is the longitudinal velocity in water and f is the ultrasonic frequency. There is a problem with the absolute value of the LSAW velocity that LSAW velocities measured for one specimen may vary depending upon the systems and ultrasonic devices used for measurements. Therefore the system was calibrated by using standard specimens of a $LiNbO_3$ or $LiTaO_3$ crystal,[13] for which the acoustical physical constants were accurately measured with an accuracy of ± 0.8 m/s.[27]

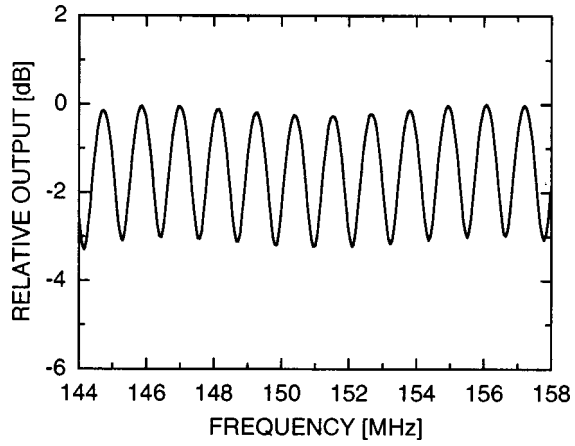

FIG. 3. Frequency characteristics of interference output for a Y-cut $LiNbO_3$ specimen in longitudinal wave velocity measurement by the pulse interference method. Melt composition: 48.5 Li_2O mol %. Specimen thickness: 2998.0 μm.

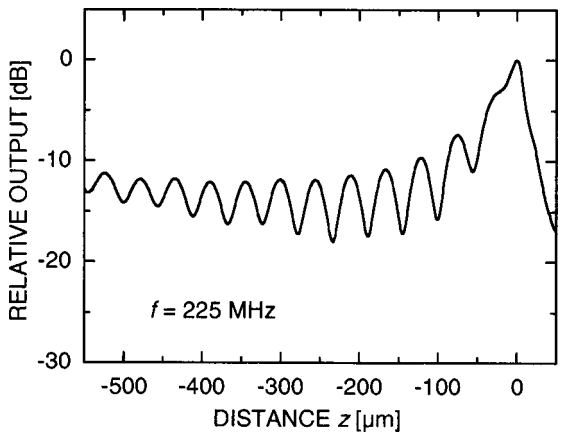

FIG. 5. V(z) curve obtained for a 128° Y X-$LiNbO_3$ specimen. Melt composition: 48.5 Li_2O mol %.

C. Dielectric constant

The dielectric constant is obtained by measuring the capacitance of a plate specimen with full electrodes prepared by depositing metal films on both sides of the specimen. If we set the measuring frequency to a value that is sufficiently lower than the lowest resonance frequency, we can accurately measure the dielectric constant at constant stress (ε^T) and then obtain the dielectric constant at constant strain (ε^S) by calculations using the following equation:[28]

$$\varepsilon_{ij}^S = \varepsilon_{ij}^T - e_{ip} s_{pq}^E e_{qj} . \tag{9}$$

Here, s^E is the elastic compliance constant and is expressed by $s^E = (c^E)^{-1}$. ε_{11}^T can be measured using an *X*-cut or *Y*-cut specimen, and ε_{33}^T by using a *Z*-cut specimen for $LiNbO_3$ and $LiTaO_3$ single crystals. The accuracy is estimated to be around $\pm 1\%$.

D. Density

The density is obtained by measuring the weight in air and in water and using the Archimedes method.[29] The accuracy is $\pm 0.005\%$.

V. RESULTS

The velocities, dielectric constants, and density of each specimen were measured around a temperature of 23.0 °C. The measured results of the *X*-axis polarized shear velocities for $LiNbO_3$ and $LiTaO_3$ crystals are shown in Figs. 6 and 7 as a function of the Li_2O content, given in Table I. Circles in the figure represent the measured results of three specimens with different compositions, and the solid line represents the straight line fitted by the least-squares method. For the $LiNbO_3$ crystals, the measured values of the *Y*-cut specimens increase linearly as the Li_2O content increases, while the values measured for the *Z*-cut and 128° *Y*-cut specimens decrease linearly. In contrast, for the $LiTaO_3$ crystals, the measured values of the shear velocities of all specimens increase linearly as the Li_2O content increases.

The velocities, dielectric constants at constant stress, and densities measured for each of the three $LiNbO_3$ and $LiTaO_3$ crystals, and the gradients of each measured parameter against the Li_2O content, are shown in Tables II and III, including the data of the shear velocities presented in Figs. 6 and 7. In Table II ($LiNbO_3$), the longitudinal velocities have positive gradients for all specimens, while the measured LSAW velocities for the *Y*-cut specimens decrease linearly and those for the *Z*-cut and 128°*Y*-cut specimens increase linearly. In Table III ($LiTaO_3$), both the longitudinal and LSAW velocities have positive gradients for all specimens. The increasing and decreasing rates of the longitudinal, shear, and LSAW velocities vary depending upon the crystal and/or specimen surface. For both the $LiNbO_3$ and $LiTaO_3$ crystals, ε_{11}^T increases linearly as the Li_2O content increases, while ε_{33}^T decreases linearly. Also, the densities decrease linearly with the Li_2O content for both the crystals. This is due to the greater molar weights of Nb_2O_5 and Ta_2O_5 than that of Li_2O.

Next, we determined all the independent components of the acoustical physical constants according to the procedure described in Sec. II using the measured results of the velocities, dielectric constants, and density of each type of crystal. Just as each measured parameter varied linearly with the chemical composition, all the acoustical physical constants also varied linearly. The constants determined for the three $LiNbO_3$ crystals and the gradients in the dependence of each constant on the Li_2O content are presented in Table IV, and those for the three $LiTaO_3$ crystals, in Table V. From both tables, we can see that only two components, c_{14}^E and e_{31}, for $LiTaO_3$ have negative values. In Table IV ($LiNbO_3$), c_{44}^E, represented in Eq. (2), has a negative gradient, corresponding to the fact that both the shear velocity and the density decrease as the Li_2O content increases. For the piezoelectric constants, e_{31} and e_{33} have negative gradients. In contrast, in Table V ($LiTaO_3$), all the elastic and piezoelectric constants except for e_{33} have positive gradients.

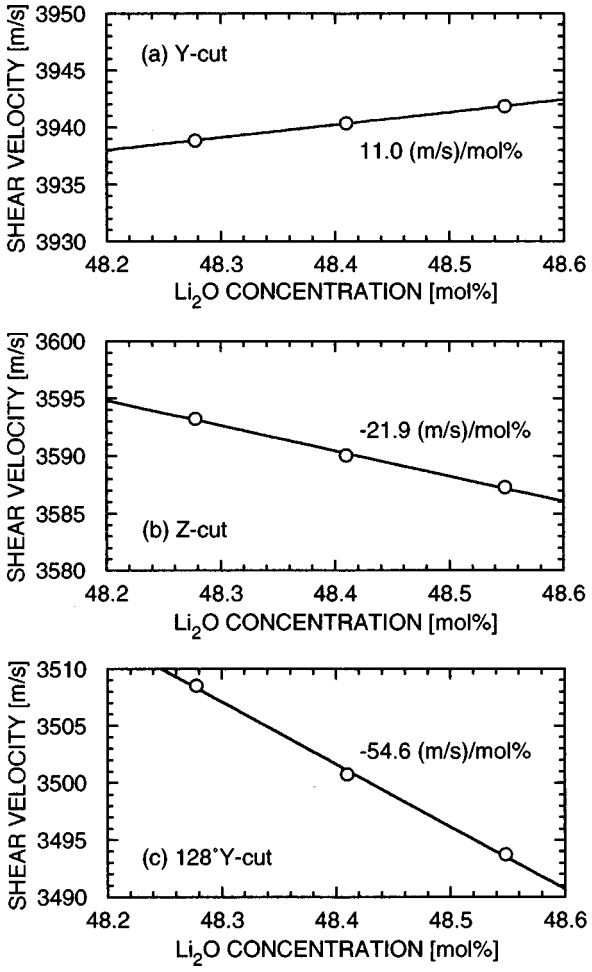

FIG. 6. Chemical composition dependences of *X*-axis polarized shear velocities of $LiNbO_3$ specimens.

VI. DISCUSSION

We calculated the chemical composition dependences of LSAW velocities using the constants in Tables IV and V for 128° *YX*-$LiNbO_3$ and *X*-112° *Y*-$LiTaO_3$, which are widely used as substrates for Rayleigh-type SAW devices, and for 36° *YX*-$LiTaO_3$ for SH-type SAW devices. The calculated results are shown by circles in Fig. 8. The solid line in the

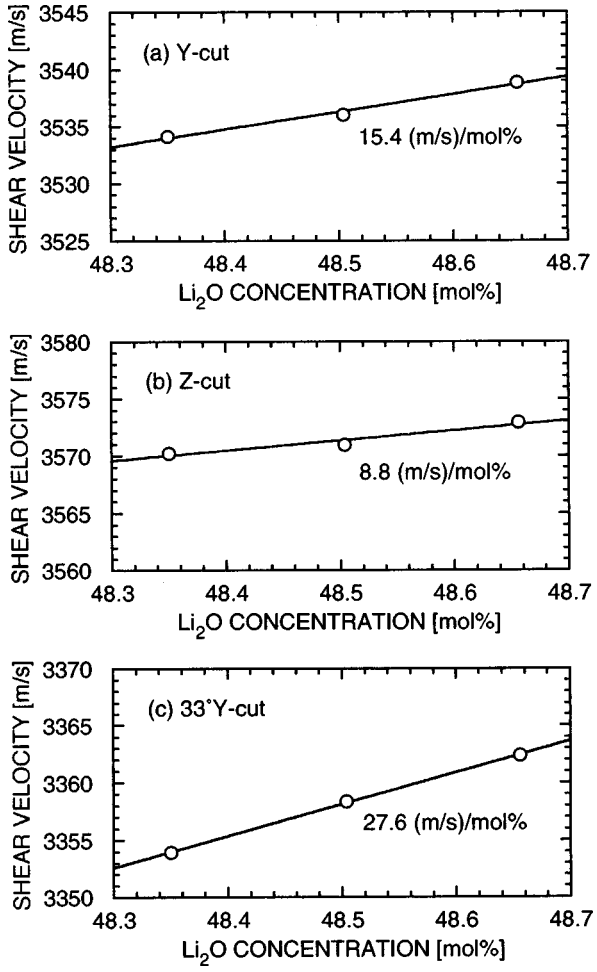

FIG. 7. Chemical composition dependences of *X*-axis polarized shear velocities of $LiTaO_3$ specimens.

figure represents the straight line fitted by the least-squares method for the three calculated results. As stated earlier, we previously obtained the experimental relations between the LSAW velocities and the chemical composition ratios.[11,17,18] The experimental data are shown in Table VI, together with the calculated results using the constants determined here. The measured and calculated values agree well within an error of about 1% for the $LiNbO_3$ substrates and about 10% for the $LiTaO_3$ substrates. This better agreement for the $LiNbO_3$ substrates than for the $LiTaO_3$ substrates may be due to the fact that the measured values for $LiNbO_3$ were obtained over a wider range of chemical compositions (47–50 Li_2O mol % in the starting material).[17] When considering the estimation error in chemical composition due to the measurement error in Curie temperature for both types of crystals, the measured values are in good agreement with the calculated values. These results indicate that the chemical composition dependences of velocities for any arbitrarily cut specimen surfaces, wave propagation directions, and modes can be obtained easily by numerical calculations using the determined constants and that these crystals can be evaluated efficiently and a feedback to the crystal growth conditions can be implemented efficiently.

Furthermore, the relationship of velocities in different modes, particularly the relationship between the LSAW velocities and SAW velocities or PSAW velocities of SH-type SAWs, can be obtained easily. Figure 9 shows the relationship between the LSAW velocities and PSAW velocities for $36°YX$-$LiTaO_3$, obtained by numerical calculations. It was previously impossible to evaluate SAW or PSAW velocities, which are related to the characteristics of the devices, directly from LSAW velocities measured by LFB acoustic microscopy. However, obtaining the calculated relationship between these two characteristics now enables us to evaluate the SAW or PSAW velocities from the measured values of the LSAW velocities.

VII. CONCLUSIONS

In this article we determined all the independent components of the acoustical physical constants of $LiNbO_3$ and $LiTaO_3$ single crystals grown from the melts of three different starting materials with the Li_2O content set to 48.0, 48.5, and 49.0 mol %. We subsequently obtained the chemical composition dependences of the constants of each crystal.

TABLE II. Chemical composition dependences of measured acoustic properties of $LiNbO_3$ crystals.

		48.28 Li_2O mol %	48.41 Li_2O mol %	48.55 Li_2O mol %	Gradient (/mol %)
Longitudinal velocity (m/s)	*X* cut	6536.7	6543.7	6550.0	48.9
	Y cut	6795.2	6805.1	6813.7	68.5
	Z cut	7322.2	7327.2	7332.0	36.3
	128°*Y* cut	7149.7	7157.8	7165.0	56.5
Shear velocity (m/s)	*Y* cut	3938.8	3940.4	3941.8	11.0
	Z cut	3593.2	3590.0	3587.3	−21.9
	128°*Y* cut	3508.5	3500.8	3493.7	−54.6
LSAW velocity (m/s)	*Y* cut	3445.6	3444.8	3443.9	−6.2
	Z cut	3868.8	3875.3	3881.3	46.1
	128°*Y* cut	3658.5	3662.1	3665.2	24.9
Dielectric constant	$\varepsilon_{11}^T/\varepsilon_0$	82.9	83.6	84.2	4.72
	$\varepsilon_{33}^T/\varepsilon_0$	28.6	28.4	28.2	−1.51
Density (kg/m^3)	ρ	4643.5	4642.8	4641.7	−6.94

TABLE III. Chemical composition dependences of measured acoustic properties of $LiTaO_3$ crystals.

		48.35 Li_2O mol %	48.50 Li_2O mol %	48.66 Li_2O mol %	Gradient (/mol %)
Longitudinal velocity (m/s)	X cut	5583.1	5588.4	5593.4	33.7
	Y cut	5738.9	5745.2	5752.6	44.6
	Z cut	6169.3	6174.5	6179.3	32.8
	33° Y cut	6324.2	6333.3	6339.8	50.9
Shear velocity (m/s)	Y cut	3534.1	3536.0	3538.9	15.4
	Z cut	3570.2	3571.0	3572.9	8.8
	33° Y cut	3353.9	3358.4	3362.4	27.6
LSAW velocity (m/s)	Y cut	3229.3	3232.0	3234.5	17.1
	Z cut	3314.3	3318.8	3322.8	28.0
	33° Y cut	3133.7	3137.7	3141.0	23.8
Dielectric constant	$\varepsilon_{11}^T/\varepsilon_0$	52.6	52.8	53.0	1.13
	$\varepsilon_{33}^T/\varepsilon_0$	43.7	43.4	43.1	−2.00
Density (kg/m^3)	ρ	7463.4	7460.6	7457.9	−18.26

TABLE IV. Chemical composition dependences of acoustical physical constants of $LiNbO_3$ crystals.

		48.28 Li_2O mol %	48.41 Li_2O mol %	48.55 Li_2O mol %	Gradient (/mol %)
Elastic constant ($\times 10^{11}$ N/m^2)	c_{11}^E	1.9844	1.9883	1.9916	0.027
	c_{12}^E	0.5433	0.5463	0.5489	0.021
	c_{13}^E	0.6794	0.6811	0.6820	0.010
	c_{14}^E	0.0758	0.0779	0.0799	0.015
	c_{33}^E	2.3382	2.3431	2.3459	0.028
	c_{44}^E	0.5996	0.5984	0.5973	−0.008
Piezoelectric constant (C/m^2)	e_{15}	3.631	3.659	3.682	0.191
	e_{22}	2.394	2.408	2.419	0.093
	e_{31}	0.332	0.328	0.320	−0.045
	e_{33}	1.896	1.878	1.870	−0.094
Dielectric constant	$\varepsilon_{11}^S/\varepsilon_0$	45.1	45.1	45.0	−0.26
	$\varepsilon_{33}^S/\varepsilon_0$	26.8	26.6	26.5	−1.33
Density (kg/m^3)	ρ	4643.5	4642.8	4641.7	−6.94

TABLE V. Chemical composition dependences of acoustical physical constants of $LiTaO_3$ crystals.

		48.35 Li_2O mol %	48.50 Li_2O mol %	48.66 Li_2O mol %	Gradient (/mol %)
Elastic constant ($\times 10^{11}$ N/m^2)	c_{11}^E	2.3264	2.3300	2.3333	0.022
	c_{12}^E	0.4620	0.4643	0.4653	0.011
	c_{13}^E	0.8356	0.8341	0.8358	0.000
	c_{14}^E	−0.1077	−0.1061	−0.1054	0.008
	c_{33}^E	2.7530	2.7574	2.7614	0.027
	c_{44}^E	0.9513	0.9514	0.9521	0.002
Piezoelectric constant (C/m^2)	e_{15}	2.609	2.634	2.650	0.132
	e_{22}	1.818	1.826	1.844	0.084
	e_{31}	−0.143	−0.090	−0.114	0.094
	e_{33}	1.804	1.792	1.779	−0.080
Dielectric constant	$\varepsilon_{11}^S/\varepsilon_0$	41.7	41.7	41.7	0.00
	$\varepsilon_{33}^S/\varepsilon_0$	41.9	41.7	41.4	−1.70
Density (kg/m^3)	ρ	7463.4	7460.6	7457.9	−18.26

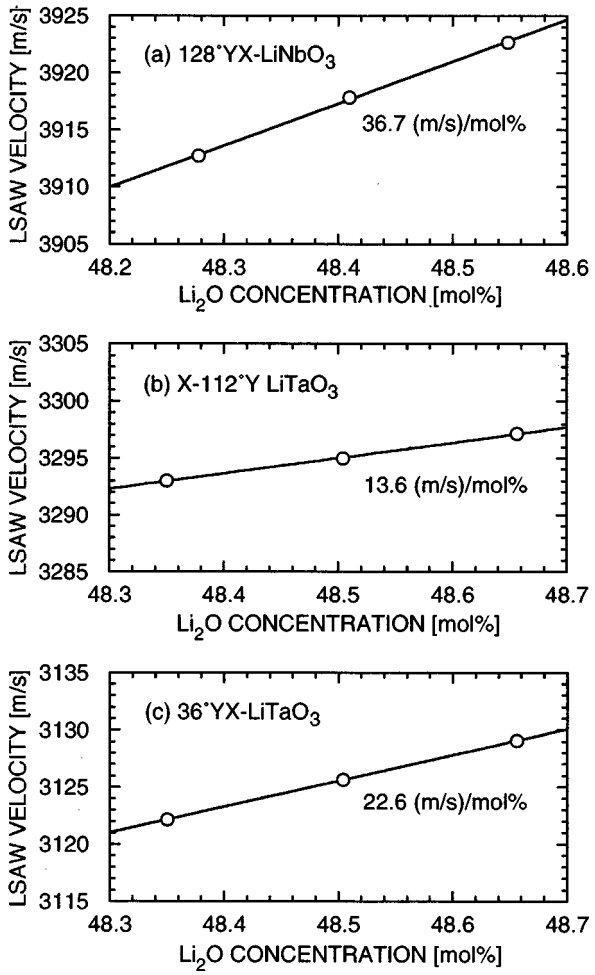

FIG. 8. Calculated chemical composition dependences of LSAW velocities for three typical substrates for SAW devices.

Within the range of nearly congruent chemical compositions employed here, all of the velocities, dielectric constants, and densities that were measured to determine the constants varied linearly with the chemical composition, and, as a result, all the constants varied linearly. The chemical composition dependences of LSAW velocities calculated for typical substrates, such as 128°YX $LiNbO_3$, X-112°Y $LiTaO_3$, and 36°YX $LiTaO_3$, which are widely used for SAW devices, using the constants determined were in good agreement with the experimental ones reported previously. The chemical composition dependences of the acoustical physical constants determined from these results enabled us to obtain the chemical composition dependences of the velocities for any arbitrarily cut crystalline surfaces, wave propagation directions, and modes by numerical calculations, eliminating the need to conduct laborious and expensive experiments for which a series of crystals with different compositions must be prepared. Therefore the acoustical characteristics of these $LiNbO_3$ and $LiTaO_3$ crystals can be evaluated very efficiently.

TABLE VI. Measured and calculated chemical composition dependences of LSAW velocities for three typical substrates for SAW devices.

	Measured	Calculated
128°YX-$LiNbO_3$	37.2 (Ref. 17)	36.7
X-112°Y $LiTaO_3$	15.2 (Ref. 11)	13.6
36°YX-$LiTaO_3$	20.1 (Ref. 18)	22.6

Unit: (m/s)/Li_2O mol %.

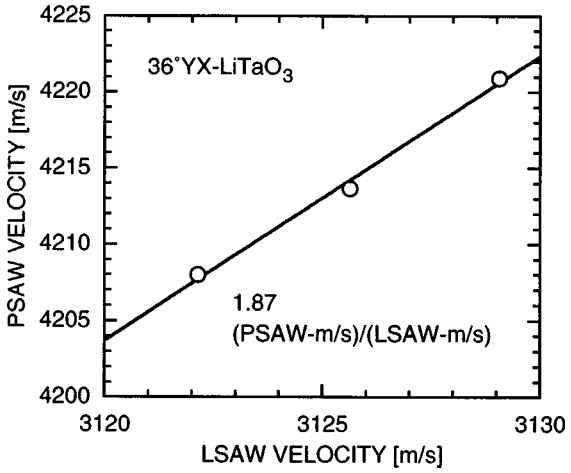

FIG. 9. Calculated relationship between LSAW velocities and PSAW velocities for a 36°Y X-$LiTaO_3$ substrate.

Thus we have completed a method for evaluating inhomogeneities in acoustic properties among crystal ingots and wafers of $LiNbO_3$ and $LiTaO_3$ single crystals due to the chemical composition changes, based on measuring the velocities, such as the BAW velocities, LSAW velocities obtained by the LFB-UMC system, and SAW velocities measured by fabricating interdigital transducers on the substrates.

The LFB-UMC system has been successfully applied not only to standardized evaluation of the chemical composition of $LiNbO_3$ and $LiTaO_3$ wafers for SAW devices[11,30] but also to evaluation and improvement of optical-grade $LiTaO_3$ crystals.[10,31] Studies will be further extended to characterization and evaluation of stoichiometric $LiNbO_3$ and $LiTaO_3$ crystals destined for optical use which are grown by the double-crucible Czochralski technique.[32,33]

ACKNOWLEDGMENTS

The authors are grateful to T. Sasamata of Yamaju Ceramics Co., Ltd. for growing the crystals and measuring the Curie temperatures, and to Y. Okada of Kogakugiken Co., Ltd. for preparing the specimens. This work was supported in part by the Research Grants-in-Aid from the Ministry of Education, Science, and Culture of Japan, and from the Japan Society for the Promotion of Science for the Research for the Future Program.

[1] A. A. Ballman, J. Am. Ceram. Soc. **48**, 112 (1965).
[2] J. R. Carruthers, G. E. Peterson, M. Grasso, and P. M. Bridenbaugh, J. Appl. Phys. **42**, 1846 (1971).
[3] R. L. Barns and J. R. Carruthers, J. Appl. Crystallogr. **3**, 395 (1970).
[4] S. Miyazawa and H. Iwasaki, J. Cryst. Growth **10**, 276 (1971).
[5] J. Kushibiki and N. Chubachi, IEEE Trans. Sonics Ultrason. **SU-32**, 189 (1985).
[6] J. Kushibiki, Y. Ono, Y. Ohashi, and M. Arakawa, IEEE Trans. Ultrason. Ferroelectr. Freq. Control **49**, 99 (2002).
[7] J. Kushibiki, N. Akashi, T. Sannomiya, N. Chubachi, and F. Dunn, IEEE

Trans. Ultrason. Ferroelectr. Freq. Control **42**, 1028 (1995).
[8] J. Kushibiki and M. Arakawa, J. Acoust. Soc. Am. **108**, 564 (2000).
[9] J. Kushibiki, Y. Ono, and I. Takanaga, Trans. Inst. Electron. Inf. Commun. Eng. C-I, **J82-C-I**, 715 (1999).
[10] J. Kushibiki, T. Okuzawa, J. Hirohashi, and Y. Ohashi, J. Appl. Phys. **87**, 4395 (2000).
[11] J. Kushibiki, Y. Ohashi, and Y. Ono, IEEE Trans. Ultrason. Ferroelectr. Freq. Control **47**, 1068 (2000).
[12] J. Kushibiki and N. Chubachi, *Ultrasonics International 91 Conference Proceedings* (Butterworth and Heinemann, Oxford, 1991), pp. 1–13.
[13] J. Kushibiki, I. Takanaga, M. Arakawa, and T. Sannomiya, IEEE Trans. Ultrason. Ferroelectr. Freq. Control **46**, 1315 (1999).
[14] K. Shibayama, K. Yamanouchi, H. Sato, and T. Meguro, Proc. IEEE **64**, 595 (1976).
[15] H. Hirano, T. Fukuda, S. Matsumura, and S. Takahashi, *Proceedings of the First Meeting on Ferroelectric Materials and Their Applications*, Kyoto, Japan (1978), pp. 81–86.
[16] K. Nakamura, M. Kazumi, and H. Shimizu, *IEEE Ultrasonics Symposium Proceedings*, Phoenix, AZ (IEEE, New York, 1977), pp. 819–822.
[17] J. Kushibiki, H. Takahashi, T. Kobayashi, and N. Chubachi, Appl. Phys. Lett. **58**, 2622 (1991).
[18] J. Kushibiki, H. Ishiji, T. Kobayashi, N. Chubachi, I. Sahashi, and T. Sasamata, IEEE Trans. Ultrason. Ferroelectr. Freq. Control **42**, 83 (1995).
[19] A. W. Warner, M. Onoe, and G. A. Coquin, J. Acoust. Soc. Am. **42**, 1223 (1967).
[20] R. T. Smith and F. S. Welsh, J. Appl. Phys. **42**, 2219 (1971).
[21] G. Kovacs, M. Anhorn, H. E. Engan, G. Visintini, and C. C. W. Ruppel, *IEEE Ultrasonics Symposium Proceedings*, Honolulu, HI (IEEE, New York, 1990), pp. 435–438.
[22] I. Takanaga and J. Kushibiki, IEEE Trans. Ultrason. Ferroelectr. Freq. Control (to be published).
[23] J. J. Campbell and W. R. Jones, IEEE Trans. Sonics Ultrason. **SU-17**, 71 (1970).
[24] K. Yamada, H. Takemura, Y. Inoue, T. Omi, and S. Matsumura, Jpn. J. Appl. Phys., Part 1 **26-2**, 219 (1987).
[25] M. Sato, A. Iwama, J. Yamada, M. Hikita, and Y. Furukawa, Jpn. J. Appl. Phys., Part 1 **28-1**, 111 (1989).
[26] J. Kushibiki, Y. Ohashi, and M. Arakawa, IEEE Trans. Ultrason. Ferroelectr. Freq. Control **47**, 274 (2000).
[27] J. Kushibiki and M. Arakawa, IEEE Trans. Ultrason. Ferroelectr. Freq. Control **45**, 421 (1998).
[28] IEEE Standard on Piezoelectricity, Std 176–1987.
[29] H. A. Bowman and R. M. Schoonover, J. Res. Natl. Bur. Stand. **71C**, 179 (1967).
[30] J. Kushibiki, Y. Ohashi, and T. Ujiie, IEEE Trans. Ultrason. Ferroelectr. Freq. Control (to be published).
[31] J. Kushibiki, Y. Ohashi, Y. Ono, and T. Sasamata, IEEE Trans. Ultrason. Ferroelectr. Freq. Control (to be published).
[32] K. Kitamura, J. K. Yamamoto, N. Iyi, S. Kimura, and T. Hayashi, J. Cryst. Growth **116**, 327 (1992).
[33] Y. Furukawa, K. Kitamura, E. Suzuki, and K. Niwa, J. Cryst. Growth **197**, 889 (1999).